ResearchGate

See discussions, stats, and author profiles for this publication at: https://www.researchgate.net/publication/282133704

Hierarchical CuO–TiO2 Hollow Microspheres for Highly Efficient Photodriven Reduction of CO2 to CH4

ARTICLE *in* ACS SUSTAINABLE CHEMISTRY & ENGINEERING · SEPTEMBER 2015

Impact Factor: 4.64 · DOI: 10.1021/acssuschemeng.5b00724

READS

57

5 AUTHORS, INCLUDING:

Baizeng Fang

University of British Columbia - Vancouver

101 PUBLICATIONS **2,236** CITATIONS

SEE PROFILE

Yalan Xing

Beihang University(BUAA)

28 PUBLICATIONS **201** CITATIONS

SEE PROFILE

Arman Bonakdarpour

University of British Columbia - Vancouver

50 PUBLICATIONS **1,577** CITATIONS

SEE PROFILE

Available from: Baizeng Fang
Retrieved on: 02 February 2016

ACS Sustainable Chemistry & Engineering

Research Article

pubs.acs.org/journal/ascecg

Hierarchical CuO–TiO_2 Hollow Microspheres for Highly Efficient Photodriven Reduction of CO_2 to CH_4

Baizeng Fang,[†] Yalan Xing,[†,‡] Arman Bonakdarpour,[†] Shichao Zhang,[*,‡] and David P. Wilkinson[*,†]

[†]Department of Chemical & Biological Engineering, University of British Columbia, 2360 East Mall, Vancouver, British Columbia V6T 1Z3, Canada

[‡]School of Materials Science and Engineering, Beihang University, 37 Xueyuan Road, Beijing 100191, People's Republic of China

Supporting Information

ABSTRACT: In this study, a scalable one-pot template-free synthesis strategy was employed to fabricate CuO-incorporated TiO_2 hollow microspheres in large scale. The as-prepared hollow spherical TiO_2 nanoparticles possess unique structural characteristics, namely, large surface area and a hierarchical nanoarchitecture composed of a hollow macroporous core connected with large mesopores in the shell. The large surface area provides a great number of surface active sites for the reactant adsorption and reaction whereas the hierarchical nanoarchitecture enables fast mass transport of reactant and product molecules within the porous framework. In addition, the hollow macroporous core–mesoporous shell nanostructure favors multilight scattering/reflection, resulting in enhanced harvesting of exciting light. Furthermore, the incorporated CuO clusters work efficiently as a cocatalyst to improve the photocatalytic activity. As a result, the CuO-incorporated TiO_2 hollow microsphere catalyst demonstrates much higher photocatalytic activity toward photodriven reduction of CO_2 with H_2O into CH_4 compared with the state-of-the-art photocatalyst, commercial Degussa P25 TiO_2. Also, the simple synthesis strategy would enable large-scale industrial production of CuO–TiO_2 hollow microspheres.

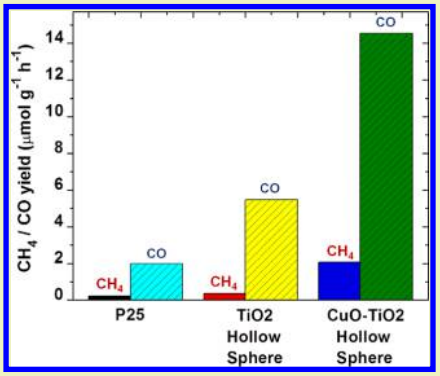

KEYWORDS: *Hierarchical nanoarchitecture, Hollow microspheres, CuO, Titania, Photocatalytic CO_2 reduction*

INTRODUCTION

In the past decades, a lot of effort has been devoted to finding ways to reduce the problem of the greenhouse gas, CO_2, which results in global climate change. One approach would be to turn CO_2 into a clean energy fuel, thus reducing the use of fossil fuels and reducing global warming as well. However, the process for turning CO_2 into fuels is energy intensive and useful only if a renewable energy source can be used for that purpose. Solar energy has proved to be one of the best renewable choices because it is clean and inexhaustible. Thus, photocatlytic conversion of CO_2 into hydrocarbon fuels is considered to be a promising avenue for sustainable development.

To date, various semiconductors and hybrids have been investigated for photocatalytic reduction of CO_2, including rhenium(I) complexes,[1] CdS,[2,3] nontitanium metal oxides and sulfides,[4] titanium metal–organic frameworks,[5] ZrO_2,[6] $ZnGa_2O_4$,[7] $SrTiO_3$,[8] WO_3,[9] CuO–$TiO_{2-x}N_x$,[10] CuO–Cu_2O,[11] CuO–ZnO,[12] Co–TiO_2,[13] Co complex–TiO_2,[14] La–TiO_2,[15] In–TiO_2,[16] MgO–TiO_2,[17] $Ca_xTi_yO_3$,[18] CdS–TiO_2,[19] etc. Among various semiconductors, titania has been exclusively considered to be an ideal candidate for photocatalytic processes due to its powerful oxidation ability, superior charge transfer characteristics, long-term stability against photo- and chemical corrosion, nontoxicity, high availability, and low production cost.[20−38] Various TiO_2 based materials have been examined for photodriven CO_2 conversion,[39−41] but to date mainly commercial Degussa P25 has been used.[42−44] TiO_2 nanotubes (NTs) have also been investigated for photodriven CO_2 conversion.[45,46] However, the high cost for the fabrication of high performance TiO_2 NTs limits their practical application greatly.

Incorporating transition metals has proven to be an effective strategy to tailor the structure, phase, and band gap of TiO_2 based photocatalysts. Among them, copper is considered to be one of the most suitable elements due to the narrower band gap of cupric oxide and cuprous oxide.[47] In addition, cupric and cuprous oxides and metallic copper are almost nontoxic. TiO_2 based photocatalysts with various copper species (i.e., Cu(0), Cu(I) and Cu(II)) have been prepared,[48] and various synthesis methods such as the impregnation method[48] and the sol–gel method[49−51] were investigated. It was reported that the Cu(II) doped TiO_2 catalyst performs better than Cu(0) or Cu(I) doped ones.[48]

Nanostructured materials with hollow macroporous cores and mesoporous shells have attracted much attention due to their unique structural characteristics. These characteristics include a large surface area, which provides a large quantity of active sites for the adsorption and reaction of reactants, a hollow macroporous core that is open and connected with the mesopores in the shell, serving as an electrolyte reservoir to

Received: March 18, 2015
Revised: September 2, 2015

ACS Publications © XXXX American Chemical Society

DOI: 10.1021/acssuschemeng.5b00724
ACS Sustainable Chem. Eng. XXXX, XXX, XXX–XXX

minimize the diffusion distance to the interior surface of the mesoporous shell, and the mesoporous channels in the shell open and connected with the macroporous core, forming fast mass transport networks around the micropores in the shell, and providing sites for diffusion and adsorption of reactant molecules.[52−58] For photocatalysis, photocatalysts with a hollow interior nanostructure (i.e., hollow core, hollow channel, etc.) have additional advantages such as enhanced light harvesting due to improved multilight scattering/reflection.[59,60] Therefore, based on the above analysis, a Cu(II) doped TiO_2 hollow microsphere catalyst is expected to perform better than a conventional nanoparticle (NP) catalyst like the P25 NP catalyst.

Template methods have been widely used to fabricate porous materials with a hollow structure.[61−67] However, the creation and removal of templates is generally time-consuming and not economical. A simple template-free method is thus highly desirable for large scale synthesis. Recently, much effort has been devoted to the development of template-free methods for the fabrication of hollow structures.[29,68]

In this study, a one-pot template-free strategy was explored to prepare Cu(II)-incorporated TiO_2 hollow microspheres. The synthesis strategy is simple, reproducible, and economical, and practical for large scale production. The as-synthesized TiO_2 hollow microspheres and the CuO doped ones were explored as photocatalysts for photodriven CO_2 reduction for the first time. TiO_2 has long-term stability against photo- and chemical corrosion and particularly importantly it is nontoxic, and thus it does not impose a negative effect to the environment, which may be a big concern for some virulent semiconductor materials such as CdS.[2,3] In addition, as a cocatalyst, CuO is not only much cheaper compared with noble metals such as Pt[26] but also nontoxic. Furthermore, the issue regarding aggregation of nanoparticles with small particle size (e.g., Degussa P25),[48] which reduces the specific surface area and reactive sites, can also be effectively avoided by using a TiO_2 hollow microsphere with much larger particle size (around several hundreds of nanometers). Compared with the state-of-the-art photocatalyst, commercial Degussa P25 nanoparticle,[48] the TiO_2 hollow microsphere catalyst has a larger surface area that provides a greater number of surface active sites for the reactant adsorption and reaction whereas the hierarchical nanoarchitecture enables faster mass transport of reactant and product molecules within the porous framework. In addition, the incorporated CuO clusters work efficiently as a cocatalyst to improve further the photocatalytic activity. As a result, the as-developed CuO−TiO_2 hollow microsphere catalyst demonstrates much higher photocatalytic activity toward the photodriven reduction of CO_2 into CH_4 compared with P25 TiO_2. Furthermore, after heat treatment in an inert (Ar) or reducing atmosphere (H_2) at an elevated temperature (250 °C), the photocatalytic conversion of CO_2 to CH_4 can be further enhanced.

EXPERIMENTAL SECTION

Preparation of Photocatalysts. CuO−TiO_2 hollow microsphere catalysts were prepared by a modified one-pot template-free strategy,[68] as illustrated in Figure 1. For a typical synthesis, 1 mL of titanium(IV) oxysulfate (15 wt % solution in 1 M sulfuric acid, Sigma-Aldrich) was added into 50 mL of DI water followed by the addition of 5 mL of 0.5 M NH_4F. After the solution was stirred for several minutes, an appropriate amount of 0.05 M $CuCl_2$ aqueous solution was added to control the CuO content in the CuO-incorporated catalysts at 1, 2, 3, 4, 5, and 10 wt %. Then the mixed solution was transferred to an autoclave with a 100 mL Teflon-liner. Next, DI water was added to bring the total volume of the solution to 80 mL. The autoclave was heated in an oven to 180 °C and kept at this temperature for 20 h. After the solution cooled down to room temperature, it was heated at 100 °C overnight to remove all the water. The remaining powder was collected and calcined at 500 °C for 30 min. For comparison, plain TiO_2 hollow microspheres without Cu(II) doping were also prepared using similar procedures. In addition, to investigate the influence of Cu valence on the photocatalytic reduction of CO_2, the CuO(3 wt %)−TiO_2 hollow microsphere catalyst, which reveals the highest CH_4 yield (as discussed later), was heat-treated in an inert (i.e., Ar) or reducing atmosphere (10%H_2−N_2) at an elevated temperature (250 °C) for 3 h to produce Cu_2O−TiO_2 or Cu−TiO_2 catalysts.[61] Other transition metals such as Co were also investigated for the comparison with Cu-doped TiO_2 catalyst. The Co−TiO_2 catalyst was prepared by a similar protocol to Cu−TiO_2, except $CoCl_2$ was used as the precursor in the synthesis.

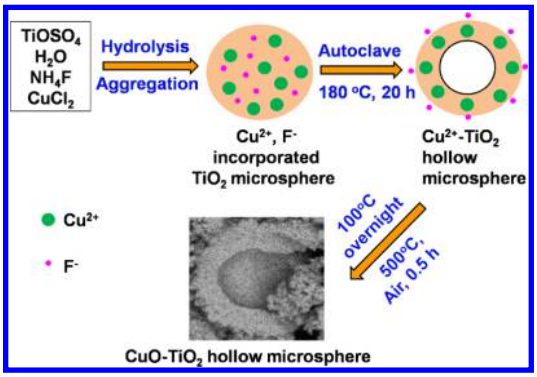

Figure 1. Schematic illustration for the synthesis of CuO−TiO_2 hollow microspheres.

Surface Characterization. Various techniques have been utilized to characterize the as-prepared TiO_2 hollow microsphere catalysts. Scanning electron microscopy (SEM) and scanning transmission electron microscopy (STEM) were used to explore the surface morphologies of the various TiO_2 based catalysts, which were performed with a FEI Helios NanoLab 650 FIB-SEM. CuO contents and elemental mapping in the CuO−TiO_2 catalysts were determined by energy dispersive X-ray spectroscopy (EDS). For the catalyst with 3 wt % (nominal value) of CuO, the content was determined to be ca. 2.9 wt %.

N_2 adsorption and desorption isotherms were measured at 77 K with a Micromeritics ASAP-2020 gas adsorption analyzer after the sample was degassed at 423 K to 20 mTorr for 12 h. The specific surface area was determined from nitrogen adsorption using the Brunauer−Emmett−Teller (BET) method. Total pore volume (V_{Total}) was determined from the amount of gas adsorbed at a relative pressure of 0.99. Micropore volume (V_{Micro}) and micropore size of the porous material were calculated from the analysis of the adsorption isotherms using the Horvath−Kawazoe (HK) method. Pore size distribution (PSD) was calculated from the adsorption branch by the Barrett−Joyner−Halenda (BJH) method.

X-ray diffraction (XRD) patterns were obtained on a Siemens D5000 (Vantec detector) and Bruker D8 Focus (LynxEye detector) X-ray powder diffractometer by using Co Kα radiation as the X-ray source, operated at 35 kV and 40 mA. The diffractograms were recorded in the 2θ range of 10−80°, in steps of 0.02° with a count time of 20 s at each point. The particle size was determined from the broadening of the diffraction peak using the Scherrer formula, $D = K\lambda/\beta \cos\theta$, where D is the crystallite size (nm), K the Scherrer constant, λ the wavelength of the X-ray source, β the full width at half-maximum, and θ the Bragg angle.

X-ray photoelectron spectroscopy (XPS) measurements were conducted in a Leybold MAX200 spectrometer using an Mg Kα source (1253.6 eV) operated at 15 kV and 20 mA. All binding energies

DOI: 10.1021/acssuschemeng.5b00724
ACS Sustainable Chem. Eng. XXXX, XXX, XXX−XXX

were corrected for sample charging by referencing to the adventitious C 1s peak at 285.0 eV.

A Varian Cary 100 UV−visible diffuse reflectance spectrophotometer was employed to obtain UV−visible diffuse reflectance spectra (UV−vis DRS) for various photocatalysts over a spectral range of 200−800 nm.

Photodriven Reduction of CO_2. Water was used as the only electron donor because the use of titania and water ultimately provides a green chemistry approach for the photoconversion of CO_2 to fuels.[26]

A batch reactor with a diameter of 39 mm and a depth of 9 mm was built for photocatalytic conversion of CO_2 under the aid of water. For a typical run, 10 mg of catalyst was mixed with 200 μL of H_2O and the paste was uniformly spread on the bottom of a container (20 mm in diameter) located in the center of the reactor. After the introduction of pressurized CO_2 (50 PSI) (or N_2, for blank experiments only), the reactor was irradiated under a Hg UV lamp (40 W; 254 nm; light intensity at the location of the catalyst: 20 mW cm^{-2}) for a 24 h period. Next, the gas products were collected through a 10 mL syringe and injected into a gas chromatograph (SRI 8610 gas chromatograph, Mandel, Canada), which was equipped with FID and TCD detectors for the detection of CH_4, CO, and H_2, respectively. Because this study focused on CO_2 photoreduction on a gas−solid interface, possible liquid products like methanol, formaldyhyde and formic acid, which are more likely generated in aqueous solutions,[26] were not measured. For each type of catalyst, experiments were carried out at least three times using fresh catalyst each time. The production rates are averaged and reported with standard deviations.

Stability tests were conducted with the used photocatalysts after being removed from the reactor followed by storage in air at ambient conditions for 24 h. Then, the used photocatalysts were placed back in the reactor without further treatment.

Prior to any photocatalytic conversion of CO_2 with water, blank experiments were performed for all of the reported catalysts to ensure there was no carbon-containing product produced without introduction of CO_2 into the reactor. The results from the blank experiments confirmed that the carbon-containing gas products (i.e., CO, CH_4, etc.) were produced from the photodriven conversion of CO_2 only, rather than from any residual carbon-containing organics in the catalysts.

RESULTS AND DISCUSSION

SEM images shown in Figure 2 reveal that the as-prepared TiO_2 microspheres are basically monodispersed (separate) and uniform in particle size, and from the broken spheres a hollow macroporous core can be clearly seen. Generally, the microspheres are produced uniformly with a particle size of ca. 1000 nm although some of them agglomerate together to form larger particle sizes (greater than 1500 nm). The shell has a thickness of ca. 110 nm. In addition, mesopores/macropores can be viewed in the shell from the rough surface, as shown in Figure 2C.

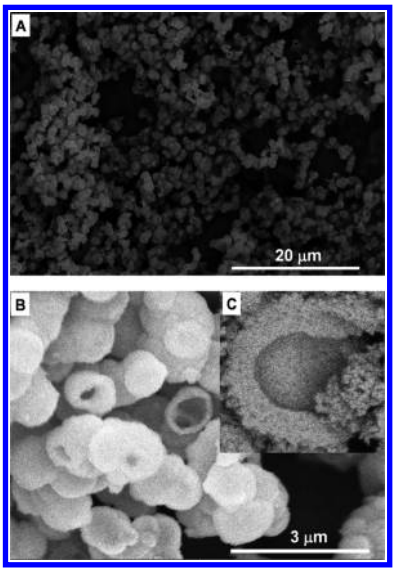

Figure 2. SEM images with various magnifications (A, B, and C) for the as-prepared TiO_2 hollow microspheres.

The hollow macroporous core/mesoporous shell nanostructure is supposed to provide the TiO_2 hollow microspheres with a large BET specific surface area and mesoporous volume. The N_2 adsorption−desorption isotherms measurement, as shown in Figure 3, reveals a BET surface area of ca. 87.3 m^2 g^{-1} and a mesoporous volume of ca. 0.387 m^3 g^{-1} for the as-prepared TiO_2 hollow microspheres. In addition, the adsorption−desorption isotherms show the characteristic of a type IV isotherm with a type H3 hysteresis loop,[26,70] indicating the presence of mesopores in the size range 2−50 nm, which is consistent with that observed from the SEM images. Furthermore, the hysteresis loop shifts to a higher relative pressure on approaching $P/P_0 \approx 1$, implying that macropores (>50 nm) are also present.[65,68] This is also evident from the PSD in Figure 3, which displays a PSD maximum located at ca. 15 nm along with macropores. Compared with Degussa P25 TiO_2, which has a BET surface area of ca. 48.4 m^2 g^{-1} and a mesoporous volume of 0.180 m^3 g^{-1},[21] the as-prepared TiO_2 hollow microspheres have a significantly larger surface area and mesoporous volume, resulting mainly from the hollow core/mesoporous shell nanostructure. These unique structural characteristics including large surface area and mesoporous volume, and particularly the hollow macroprous core that is open and connected with the mesopores in the shell are expected to improve the photocatalytic activity toward photodriven CO_2 conversion to fuels.

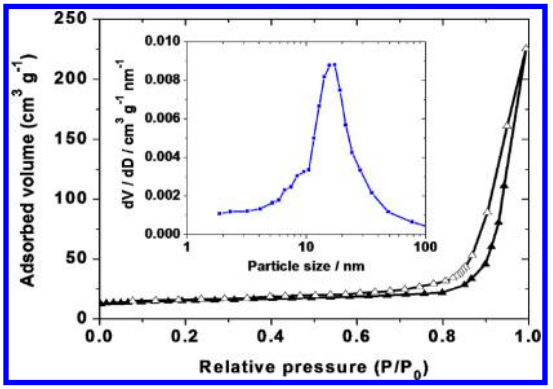

Figure 3. Nitrogen adsorption−desorption isotherms at 77 K and the derived PSD for the as-prepared TiO_2 hollow microspheres.

Various amounts of CuO were incorporated *in situ* into the TiO_2 hollow microspheres in order to improve further the photocatalytic conversion efficiency of CO_2. The XRD patterns shown in Figure 4 reveal that the plain TiO_2 hollow microspheres are mainly composed of pure anatase phase, which is consistent with results reported previously.[68] The CuO (3 wt %)-incorporated sample demonstrates a similar pattern, and no Cu species peak was observed. This phenomenon was also observed for Cu-incorporated TiO_2 materials when Cu contents were lower than 3 wt %.[48,49,51] Diffraction peaks for copper species were not detected, implying that they are highly

DOI: 10.1021/acssuschemeng.5b00724
ACS Sustainable Chem. Eng. XXXX, XXX, XXX−XXX

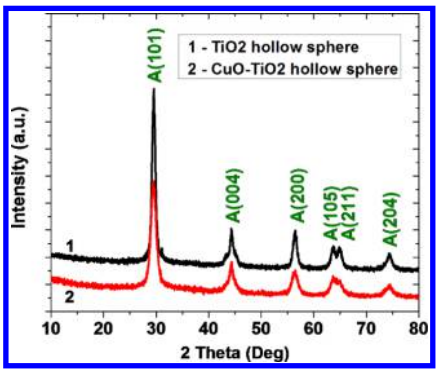

Figure 4. XRD patterns for the plain TiO_2 hollow microsphere and CuO (3 wt %)-incorporated one.

dispersed or it is due to the low Cu(II) concentration and extremely small CuO clusters.[49,51] In addition, this result also suggests that the incorporation of Cu with low loading does not affect the crystalline structure of the TiO_2 hollow microspheres. Interestingly, with a high CuO loading (e.g., 10 wt %), a peak located at ca. 35.6° is clearly observed, as shown in Figure S1 (Supporting Information), implying the presence of crystalline CuO.

Figure 5 shows representative XPS spectra for the as-synthesized TiO_2 hollow microspheres and CuO(3 wt

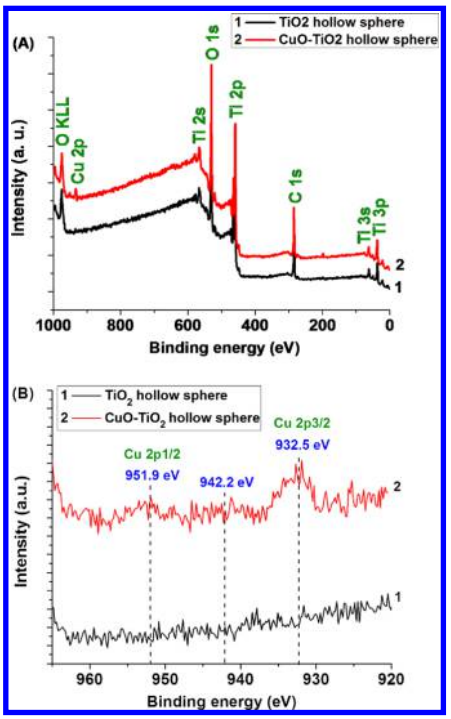

Figure 5. XPS survey spectra (A) and the high-resolution spectra of Cu 2p doublet (B) for the plain TiO_2 hollow microsphere and CuO(3 wt %)-incorporated TiO_2 hollow microsphere.

%)-incorporated TiO_2 hollow microspheres. For the CuO(3 wt %)-incorporated sample, the peaks for Cu $2p_{1/2}$ and $2p_{3/2}$ are clearly observed. In addition, even for a TiO_2 hollow microsphere sample with a lower CuO content (e.g., 1 wt %), the peaks for Cu $2p_{1/2}$ and $2p_{3/2}$ can be seen, as shown in Figure S2 (Supporting Information).

The binding energies of Cu $2p_{3/2}$ and $2p_{1/2}$ were found to be 932.5 and 951.9 eV, respectively, suggesting that the dominant species in the samples is Cu(II).[71] In addition, the molar ratio of Cu/Ti was found to be 0.051, higher than the bulk Cu/Ti molar ratio calculated (i.e., 0.025), implying that CuO is dispersed mostly on the surface of the CuO-incorporated catalyst.[50] Figures S3 and S4 (Supporting Information) show representative STEM images and elemental mapping, respectively, for the CuO(3 wt %)-incorporated TiO_2 hollow microspheres. From Figure S3 (Supporting Information), it is clear that even after the CuO incorporation TiO_2 microspheres still remain a hollow nanostructure, whereas the elemental mapping shown in Figures S4 (Supporting Information) suggests that the incorporated CuO nanoparticles disperse almost uniformly in the entire shell of the TiO_2 hollow microspheres.

Figure 6 shows typical UV−vis DRS for the as-synthesized TiO_2 hollow microspheres and Cu(3 wt %)-incorporated TiO_2

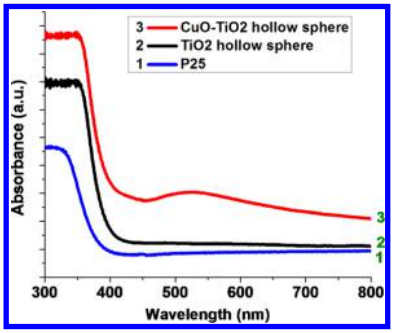

Figure 6. UV−vis DRS for various TiO_2 based nanomaterials. The CuO content in the CuO−TiO_2 catalyst is 3 wt %.

hollow microspheres. Compared with P25 TiO_2 NPs, the as-synthesized TiO_2 hollow microspheres reveal considerably enhanced photoabsorption, which is mainly attributable to the unique nanostructure of the latter, namely, the hollow macroporous core open and connected with the large mesopores/macropores in the shell. Other researchers have reported enhanced photoabsorption for hierarchical hollow nanostructures.[72] In a hollow core/mesoporous shell TiO_2 photocatalyst, the large mesopores/macropores in the shell can act as a light-transfer path allowing light to penetrate deep inside the photocatalyst. This could introduce an incident photon flux onto the inner surface of the TiO_2 catalyst, whereas the surface of the hollow core could cause light absorption, reflection, and scattering, making the catalyst a more efficient light harvester, and thus the effective light-activated surface area can be significantly enhanced.[26,72,73] It is also interesting to note that after the Cu incorporation, there is an enhanced photoabsorption in the visible-light region. However, there is no significant change in the absorption edge, suggesting that CuO is not incorporated into the lattice of TiO_2, but dispersed mainly on its surface instead.[71]

Various CuO contents for the TiO_2 hollow core microsphere catalysts have been examined for photodriven CO_2 conversion with the aid of water and the data are plotted in Figure 7. The plain TiO_2 hollow microsphere catalyst (i.e., CuO content = 0) reveals a H_2 yield of 1.84, CO yield of 5.47, and a CH_4 yield of 0.36 μmol g(catalyst)$^{-1}$ h^{-1}, which is significantly higher than that (i.e., 0.79, 1.99, and 0.23 μmol g(catalyst)$^{-1}$ h^{-1}, respectively) produced by the P25 TiO_2 NP catalyst (data not shown in Figure 7). In other words, compared with the P25 catalyst, the yields for the gas products H_2, CO, and CH_4

DOI: 10.1021/acssuschemeng.5b00724
ACS Sustainable Chem. Eng. XXXX, XXX, XXX−XXX

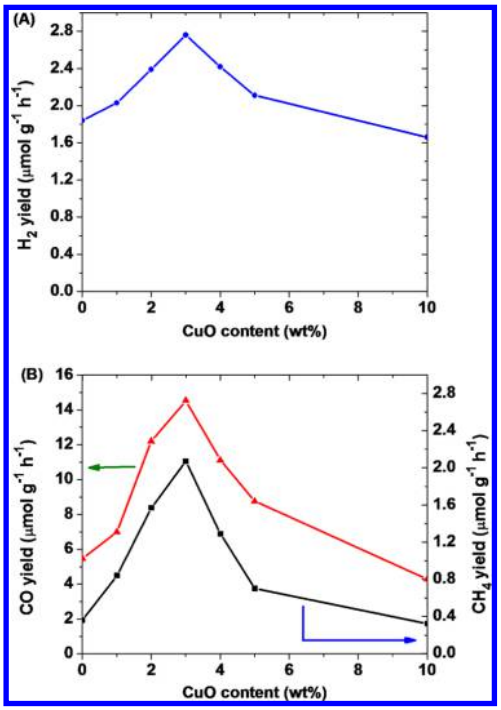

Figure 7. Yields of the gas products (H_2, CO, and CH_4) produced during 24 h of photodriven CO_2 reduction on the TiO_2 hollow microsphere catalysts with various Cu contents.

demonstrated by the plain TiO_2 hollow microsphere catalyst are ca. 2.3, 2.7, and 1.6 times greater, respectively. In both of the cases, the intermediate product CO is identified as the major carbon-containing gas product, and no C_2H_6 or ethylene or acetylene was detected, as observed by other researchers.[51] Compared with the P25 catalyst, the enhancement in the photocatalytic conversion of CO_2 is mainly attributable to the larger surface area and particularly the unique nanostructure of the TiO_2 hollow microsphere. As discussed previously, the TiO_2 hollow microsphere shows improved photoabsorption due to enhanced multilight reflection/scattering. In addition, the hierarchical nanostructure composed of the hollow macroporous core/mesoporous shell facilitates fast mass transport within the catalyst porous network, which has been reported previously.[52,53]

Compared with the plain TiO_2 hollow microsphere catalyst, the CuO incorporation increases the photoconversion of CO_2 when the CuO content is smaller than 5 wt %. A maximum CO_2 conversion was observed for the TiO_2 hollow sphere catalyst with a CuO content of ca. 3 wt %, which demonstrates a yield of ca. 2.8, 14.5, and 2.1 μmol g(catalyst)$^{-1}$ h^{-1} for the production of H_2, CO and CH_4, respectively. The yields are ca. 1.5, 5.8, and 2.7 times greater, respectively compared with that of the plain hollow TiO_2 hollow microsphere, and ca. 3.5, 7.3, and 9.0 times greater compared with that of the P25 TiO_2 NP catalyst. In addition, the yields (i.e., 14.5 and 2.1 μmol g(catalyst)$^{-1}$ h^{-1} for the production of CO and CH_4, respectively) observed from the CuO(3 wt %)/TiO_2 are comparable to that reported for the Pt(0.6 wt %)/TiO_2 ultralarge microsphere catalyst (i.e., 18.9 and 3.6 μmol g(catalyst)$^{-1}$ h^{-1} for the production of CO and CH_4, respectively).[26]

It is particularly interesting to note that after the CuO loading, the yield of CH_4 observed from the CuO(3.0 wt %)/TiO_2 hollow microsphere catalyst has increased from 1.6 to 9 times when compared with P25, whereas the yield of CO increases from 2.7 to 7.3 times, and the yield of H_2 increases from 2.3 to 3.5 times. The comparison implies that the CuO loading facilitates more CH_4 production than other gas products (i.e., CO and H_2). This phenomenon was also observed by other researchers. Li et al. reported that without Cu loading the TiO_2–SiO_2 catalyst reveals a negligible yield of CH_4 whereas after the Cu loading the yield of CH_4 increases considerably.[51] The higher selectivity of CH_4 production in the presence of Cu species is mainly attributable to the enhanced electron traps, and accordingly, the increased possibility of multielectron reactions (i.e., eight electrons for CH_4 production). Because CH_4 is the end product for the photocatalytic reduction of CO_2 with the aid of H_2O,[26] the end product has more significance than the intermediate products such as CO. The as-prepared CuO (3 wt %)–TiO_2 hollow microsphere catalyst demonstrates the highest CH_4 production yield, suggesting it is a very promising catalyst for in photodriven CO_2 conversion to fuels.

From Figure 7, it is also noted that the gas product yields show an increasing trend with the increasing CuO content until 3 wt %, and decreases with the further increase in the CuO content. Compared with the plain TiO_2 hollow microsphere catalyst (i.e., CuO content = 0), the enhanced gas product yields for the CuO-incorporated TiO_2 hollow microsphere catalysts is mainly attributed to the improved electron traps, the reduced recombination of photoinduced electrons and holes, and the enhanced photoabsorption, as evident from the UV–vis DRS shown in Figure 6. However, an excess CuO loading (more than 3 wt %) results in an uneven dispersion of CuO with larger particle size in the TiO_2 catalyst, a reduced TiO_2 surface area for the photocatalysis, and an increased possibility for excess Cu species serving as recombination centers for photogenerated electrons and holes,[51] and thus the decreased gas product yields.

Because the CuO(3 wt %)–TiO_2 reveals the highest yield of CH_4, the as-synthesized CuO(3 wt %)–TiO_2 was further heat-treated under Ar or H_2 to produce Cu_2O–TiO_2 and Cu–TiO_2, respectively.[69] CoO(3 wt %)–TiO_2 was also heat-treated under a reducing atmosphere (10%H_2–N_2) to produce Co–TiO_2. The XPS spectra for the Cu_2O–TiO_2 and Cu–TiO_2, and the Co–TiO_2 are shown in Figures S5 and S6 (Supporting Information), respectively, from which characteristic peaks for Cu or Co species can be clearly observed. Compared with the as-synthesized CuO(3 wt %)–TiO_2 catalyst, the Cu_2O–TiO_2 and Cu–TiO_2 demonstrate a further enhancement of ca. 6% and 28%, respectively in the photocatalytic reduction of CO_2 to CH_4, whereas the Co–TiO_2 shows ca. 9% improvement. The higher CH_4 yield observed for Cu^+ is probably mainly attributed to the synergy between Cu^+ species and the surface defect sites. Liu et al. reported that Cu^+ species on the catalyst surface could trap electrons more efficiently than Cu^{2+} species due to its higher reduction potential.[70] In the case of Cu–TiO_2, the abundant Cu species are supposed to facilitate the capture of photogenerated holes, favoring H_2O dissociation to supply enough protons for the CH_4 production. Compared with the Cu–TiO_2 catalyst, the Co–TiO_2 shows much less CH_4 yield probably due to its wider band gap.

The apparent quantum yield (Φ) for the gas products CO and CH_4 can be calculated according to the following equation:[26]

DOI: 10.1021/acssuschemeng.5b00724
ACS Sustainable Chem. Eng. XXXX, XXX, XXX–XXX

$$\Phi_{product}\ (\%) = (n \text{ mol product yield/moles photons absorbed by catalyst}) \times 100\%$$

where n = 2 for CO and 8 for CH_4 according to the following reactions 1 and 2 given below, respectively.

$$CO_2 + 2H^+ + 2e^- \rightarrow CO + H_2O \quad (1)$$

$$CO_2 + 8e^- + 8H^+ \rightarrow CH_4 + 2H_2O \quad (2)$$

For the P25 TiO_2 catalyst, Φ was calculated to be 0.176% and 0.083% for CO and CH_4, respectively, whereas for the plain TiO_2 hollow microsphere catalyst, Φ was calculated to be 0.475% for CO and 0.133% for CH_4, respectively. When the catalyst is loaded with 3 wt % of CuO, Φ is increased considerably up to 1.285% and 0.747% for CO and CH_4, respectively.

Stability tests were conducted with the used CuO(3 wt %)/TiO_2 photocatalyst after being removed from the reactor followed by storage in air at ambient conditions for 24 h. After storage, the photocatalyst was tested again without further treatment and produced only a slightly reduced yield (i.e., < 5% loss). These results indicate that the photocatalyst is largely regenerated during the exposure to air due to the desorption of the gas products from its surface.

CONCLUSIONS

In this study, a one-pot template-free synthesis strategy was employed to fabricate CuO-incorporated TiO_2 hollow microspheres. The as-synthesized CuO−TiO_2 hollow microspheres were explored for the first time as a catalyst for photodriven CO_2 conversion with the aid of H_2O to fuels. The as-prepared TiO_2 hollow microsphere catalyst possesses unique structural characteristics including a large surface area and a hierarchical nanostructure composed of a hollow macroporous core open and connected with a mesoporous shell. The structure provides a large surface area with active sites for the adsorption and reaction of reactants whereas the hierarchical nanoarchitecture enables fast mass transport of reactant and product molecules. Furthermore, the hollow core-mesoporous shell nanostructure favors multilight scattering within the porous framework, resulting in enhanced photoabsorption. As a result, the TiO_2 hollow microsphere catalyst demonstrates greatly improved photocatalytic activity toward CO_2 reduction. This is particular true after CuO loading of the catalyst as the photocatalytic activity is further enhanced significantly. A maximum CO_2 conversion was observed for the TiO_2 hollow sphere catalyst loaded with about 3 wt % of CuO, which reveals a yield of 14.54 and 2.07 μmol g(catalyst)$^{-1}$ h^{-1} for the production of CO and CH_4, respectively. The yields are ca. 5.8 and 2.7 times greater, respectively compared with that of the plain hollow TiO_2 hollow microsphere, and ca. 7.3 and 9.0 times greater compared with that of conventional P25 TiO_2 catalyst. Interestingly and significantly, the CuO incorporation provides the TiO_2 hollow microsphere catalyst with higher selectivity in the production of the end product CH_4. In addition, after heat treatment at 250 °C in Ar or H_2, the as-obtained Cu_2O−TiO_2 and Cu−TiO_2 catalysts demonstrates a further enhancement in photocatalytic CO_2 reduction to CH_4.

In future work, Pt or other elements, which can change the distribution of electrons and effectively prevent the electron−hole recombination, will be incorporated into the CuO−TiO_2 hollow microsphere catalyst to enhance further the photodriven CO_2 conversion. In addition, other Cu (or CuPt)-doped TiO_2 hollow nanostructures such as urchin-like TiO_2 hollow microsphere and mesoporous TiO_2 nanotubes will be explored for photocatalytic CO_2 conversion. Furthermore, nanostructured carbon materials such as multiwalled carbon nanotubes,[74] Vulcan XC-72,[75] mesoporous carbon nanofiber,[63] hollow macroporous core/mesoporous shell carbon,[76] and multimodal porous carbon[77] will be investigated as potential candidates to support nanostructured TiO_2 materials for applications in photodriven or photoelectrochemical CO_2 reduction.

ASSOCIATED CONTENT

Supporting Information

The Supporting Information is available free of charge on the ACS Publications website at DOI: 10.1021/acssuschemeng.5b00724.

XRD pattern for the CuO(10 wt %)−TiO_2 hollow microsphere photocatalyst and XPS spectra for CuO(1 wt %)−TiO_2 hollow microsphere, STEM images and elemental mapping for the CuO(3 wt %)−TiO_2 hollow microsphere, XPS spectra for Cu_2O(3 wt %)−TiO_2, Cu(3 wt %)−TiO_2, and Co(3 wt %)−TiO_2 photocatalysts (PDF).

AUTHOR INFORMATION

Corresponding Authors

*S. Zhang. E-mail: csc@buaa.edu.cn.

*D. Wilkinson. E-mail: dwilkinson@chbe.ubc.ca. Phone: +1 604-8224888.

Notes

The authors declare no competing financial interest.

ACKNOWLEDGMENTS

The authors thank Carbon Management Canada (CMC project B222) and the Pacific Institute for Climate Solutions (PICS) for financial support. SEM/STEM and EDS analyses were performed by Dr. Gethin Owen in the Centre for High-Throughput Phenogenomics at UBC, a facility supported by the Canada Foundation for Innovation, British Columbia Knowledge Development Foundation, and the UBC Faculty of Dentistry. Dr. Yalan Xing acknowledges the financial support from the China Scholarship Council.

REFERENCES

(1) Takeda, H.; Koike, K.; Inoue, H.; Ishitani, O. Development of an efficient photocatalytic system for CO_2 reduction using Rhenium(I) complexes based on mechanistic studies. *J. Am. Chem. Soc.* **2008**, *130*, 2023−2031.

(2) Fujiwara, H.; Hosokawa, H.; Murakoshi, K.; Wada, Y.; Yanagida, S.; Okada, T.; Kobayashi, H. Effect of surface structures on photocatalytic CO_2 reduction using quantized CdS nanocrystallites. *J. Phys. Chem. B* **1997**, *101*, 8270−8278.

(3) Chaudhary, Y.; Woolerton, T.; Allen, C.; Warner, J.; Pierce, E.; Ragsdale, S.; Armstrong, F. Visible light-driven CO_2 reduction by enzyme coupled CdS nanocrystals. *Chem. Commun.* **2012**, *48*, 58−60.

(4) Navalon, S.; Dhakshinamoorthy, A.; Alvaro, M.; Garcia, H. Photocatalytic CO_2 reduction using non-titanium metal oxides and sulfides. *ChemSusChem* **2013**, *6*, 562−577.

(5) Fu, Y.; Sun, D.; Chen, Y.; Huang, R.; Ding, Z.; Fu, X.; Li, Z. An amine-functionalized titanium metal−organic framework photocatalyst with visible-light-induced activity for CO_2 reduction. *Angew. Chem.* **2012**, *124*, 3420−3423.

(6) Sayama, K.; Arakawa, H. Photocatalytic decomposition of water and photocatalytic reduction of carbon dioxide over ZrO_2 Catalyst. *J. Phys. Chem.* **1993**, *97*, 531−533.

DOI: 10.1021/acssuschemeng.5b00724
ACS Sustainable Chem. Eng. XXXX, XXX, XXX−XXX

(7) Yan, S.; Ouyang, S.; Gao, J.; Yang, M.; Feng, J.; Fan, X.; Wan, L.; Li, Z.; Ye, J.; Zhou, Y.; Zou, Z. A room-temperature reactive-template route to mesoporous $ZnGa_2O_4$ with improved photocatalytic activity in reduction of CO_2. *Angew. Chem.* **2010**, *122*, 6544−6548.
(8) Halmann, M.; Ulman, M.; Aurian-Blajeni, B. Photochemical solar collector for the photoassisted reduction of aqueous carbon-dioxide. *Sol. Energy* **1983**, *31*, 429−431.
(9) Chen, X.; Zhou, Y.; Liu, Q.; Li, Z.; Liu, J.; Zou, Z. Ultrathin, single-crystal WO_3 nanosheets by two-dimensional oriented attachment toward enhanced photocatalystic reduction of CO_2 into hydrocarbon fuels under visible light. *ACS Appl. Mater. Interfaces* **2012**, *4*, 3372−3377.
(10) In, S.; Vaughn, D., II; Schaak, R. Hybrid CuO-$TiO_{2-x}N_x$ hollow nanocubes for photocatalytic conversion of CO_2 into methane under solar irradiation. *Angew. Chem., Int. Ed.* **2012**, *51*, 3915−3918.
(11) Ghadimkhani, G.; de Tacconi, N. R.; Chanmanee, W.; Janaky, C.; Rajeshwar, K. Efficient solar photoelectrosynthesis of methanol from carbon dioxide using hybrid CuO−Cu_2O semiconductor nanorod arrays. *Chem. Commun.* **2013**, *49*, 1297−1299.
(12) Subrahmanyam, M.; Kaneco, S.; Alonso-Vante, N. A screening for the photo reduction of carbon dioxide supported on metal oxide catalysts for C1−C3 selectivity. *Appl. Catal., B* **1999**, *23*, 169−174.
(13) Wang, J.; Jing, Y.; Ouyang, T.; Zhang, Q.; Chang, C. Photocatalytic reduction of CO_2 to energy products using Cu−TiO_2/ZSM-5 and Co−TiO_2/ZSM-5 under low energy irradiation. *Catal. Commun.* **2015**, *59*, 69−72.
(14) Jin, T.; Liu, C.; Li, G. Photocatalytic CO_2 reduction using a molecular cobalt complex deposited on TiO_2 nanoparticles. *Chem. Commun.* **2014**, *50*, 6221−6224.
(15) Liu, Y.; Zhou, S.; Li, J.; Wang, Y.; Jiang, G.; Zhao, Z.; Liu, B.; Gong, X.; Duan, A.; Liu, J.; Wei, Y.; Zhang, L. Photocatalytic reduction of CO_2 with water vapor on surface La-modified TiO_2 nanoparticles with enhanced CH_4 selectivity. *Appl. Catal., B* **2015**, *168−169*, 125−131.
(16) Tahir, M.; Amin, N. Indium-doped TiO_2 nanoparticles for photocatalytic CO_2 reductionwith H_2O vapors to CH_4. *Appl. Catal., B* **2015**, *162*, 98−109.
(17) Li, Q.; Zong, L.; Li, C.; Yang, J. Reprint of "photocatalytic reduction of CO_2 on MgO/TiO_2 nanotube films. *Appl. Surf. Sci.* **2014**, *319*, 16−20.
(18) Kwak, B.; Kang, M. Photocatalytic reduction of CO_2 with H_2O using perovskite $Ca_xTi_yO_3$. *Appl. Surf. Sci.* **2015**, *337*, 138−144.
(19) Ahmad Beigi, A.; Fatemi, S.; Salehi, Z. Synthesis of nanocomposite CdS/TiO_2 and investigation of its photocatalytic activity for CO_2 reduction to CO and CH_4 under visible light irradiation. *J. CO2 Util.* **2014**, *7*, 23−29.
(20) Kong, M.; Li, Y.; Chen, X.; Tian, T.; Fang, P.; Zheng, F.; Zhao, X. Tuning the relative concentration ratio of bulk defects to surface defects in TiO_2 nanocrystals leads to high photocatalytic efficiency. *J. Am. Chem. Soc.* **2011**, *133*, 16414−16417.
(21) Xie, Y.; Ding, K.; Liu, Z.; Tao, R.; Sun, Z.; Zhang, H.; An, G. In situ controllable loading of ultrafine noble metal particles on titania. *J. Am. Chem. Soc.* **2009**, *131*, 6648−6649.
(22) Woolerton, T.; Sheard, S.; Reisner, E.; Pierce, E.; Ragsdale, S.; Armstrong, F. Efficient and clean photoreduction of CO_2 to CO by enzyme-modified TiO_2 nanoparticles using visible light. *J. Am. Chem. Soc.* **2010**, *132*, 2132−2133.
(23) Sastre, F.; Corma, A.; García, H. 185 nm photoreduction of CO_2 to methane by water. Influence of the presence of a basic catalyst. *J. Am. Chem. Soc.* **2012**, *134*, 14137−14141.
(24) Wang, W.; An, W.; Ramalingam, B.; Mukherjee, S.; Niedzwiedzki, D.; Gangopadhyay, S.; Biswas, P. Size and structure matter: enhanced CO_2 photoreduction efficiency by size-resolved ultrafine Pt nanoparticles on TiO_2 single crystals. *J. Am. Chem. Soc.* **2012**, *134*, 11276−11281.
(25) Yu, J.; Liu, S.; Yu, H. Microstructures and photoactivity of mesoporous anatase hollow microspheres fabricated by fluoride-mediated self-transformation. *J. Catal.* **2007**, *249*, 59−66.
(26) Fang, B.; Bonakdarpour, A.; Reilly, K.; Xing, Y.; Taghipour, F.; Wilkinson, D. Large-scale synthesis of TiO_2 microspheres with hierarchical naostructure for highly efficient photodriven reduction of CO_2 to CH_4. *ACS Appl. Mater. Interfaces* **2014**, *6*, 15488−15498.
(27) Cai, J.; Wang, Z.; Lv, K.; Zheng, Y.; Yu, J.; Li, M. Rapid synthesis of a TiO_2 hollow microsphere assembly from hollow nanoparticles with enhanced photocatalytic activity. *RSC Adv.* **2013**, *3*, 15273−15281.
(28) Jiao, W.; Wang, L.; Liu, G.; Lu, G.; Cheng, H. Hollow anatase TiO_2 single crystals and mesocrystals with dominant {101} facets for improved photocatalysis activity and tuned reaction preference. *ACS Catal.* **2012**, *2*, 1854−1859.
(29) Liu, Z.; Bai, H.; Sun, D. Facile fabrication of hierarchical porous TiO_2 hollow microspheres with high photocatalytic activity for water purification. *Appl. Catal., B* **2011**, *104*, 234−238.
(30) Yu, J.; Xiang, Q.; Zhou, M. Preparation, characterization and visible-light-driven photocatalytic activity of Fe-doped titania nanorods and first-principles study for electronic structures. *Appl. Catal., B* **2009**, *90*, 595−602.
(31) Indrakanti, V.; Schobert, H.; Kubicki, J. Quantum mechanical modeling of CO_2 interactions with irradiated stoichiometric and oxygen-deficient anatase TiO_2 surfaces: implications for the photocatalytic reduction of CO_2. *Energy Fuels* **2009**, *23*, 5247−5256.
(32) Pan, X.; Yang, M.; Fu, X.; Zhang, N.; Xu, Y. Defective TiO_2 with oxygen vacancies: synthesis, properties and photocatalytic applications. *Nanoscale* **2013**, *5*, 3601−3614.
(33) Liu, S.; Yu, J.; Jaroniec, M. Tunable photocatalytic selectivity of hollow TiO_2 microspheres composed of anatase polyhedra with exposed {001} facets. *J. Am. Chem. Soc.* **2010**, *132*, 11914−11916.
(34) Wang, W.; Yu, J.; Xiang, Q.; Cheng, B. Enhanced photocatalytic activity of hierarchical macro/mesoporous TiO_2−graphene composites for photodegradation of acetone in air. *Appl. Catal., B* **2012**, *119*, 109−116.
(35) Ksibi, M.; Rossignol, S.; Tatibouet, J.; Trapalis, C. Synthesis and solid characterization of nitrogen and sulfur-doped TiO_2 photocatalysts active under near visible light. *Mater. Lett.* **2008**, *62*, 4204−4206.
(36) Wen, C.; Jiang, H.; Qiao, S.; Yang, H.; Lu, G. Synthesis of high-reactive facets dominated anatase TiO_2. *J. Mater. Chem.* **2011**, *21*, 7052−7061.
(37) Xiang, Q.; Yu, J.; Jaroniec, M. Graphene-based semiconductor photocatalysts. *Chem. Soc. Rev.* **2012**, *41*, 782−796.
(38) Pomoni, K.; Vomvas, A.; Trapalis, C. Transient photoconductivity of nanocrystalline TiO_2 sol-gel thin films. *Thin Solid Films* **2005**, *479*, 160−165.
(39) Yu, J.; Low, J.; Xiao, W.; Zhou, P.; Jaroniec, M. Enhanced photocatalytic CO_2-reduction activity of anatase TiO_2 by coexposed {001} and {101} facets. *J. Am. Chem. Soc.* **2014**, *136*, 8839−8842.
(40) Yuan, L.; Xu, Y. Photocatalytic conversion of CO_2 into value-added and renewable fuels. *Appl. Surf. Sci.* **2015**, *342*, 154−167.
(41) Li, X.; Wen, J.; Low, J.; Fang, Y.; Yu, J. Design and fabrication of semiconductor photocatalyst for photocatalytic reduction of CO_2 to solar fuel. *Sci. China Mater.* **2014**, *57*, 70−100.
(42) Tan, S.; Zou, L.; Hu, E. Photocatalytic production of methane and hydrogen through reduction of carbon dioxide with water using titania pellets. *Int. J. Green Energy* **2006**, *3*, 283−290.
(43) Lo, C.; Hung, C.; Yuan, C.; Wu, J. Photoreduction of carbon dioxide with H_2 and H_2O over TiO_2 and ZrO_2 in a circulated photocatalytic reactor. *Sol. Energy Mater. Sol. Cells* **2007**, *91*, 1765−1774.
(44) Tan, S.; Zou, L.; Hu, E. Photosynthesis of hydrogen and methane as key components for clean energy system. *Sci. Technol. Adv. Mater.* **2007**, *8*, 89−92.
(45) Varghese, O.; Paulose, M.; LaTempa, T.; Grimes, C. A. High-rate solar photocatalytic conversion of CO_2 and water vapor to hydrocarbon fuels. *Nano Lett.* **2009**, *9*, 731−737.
(46) Roy, S.; Varghese, O.; Paulose, M.; Grimes, C. Toward solar fuels: photocatalytic conversion of carbon dioxide to hydrocarbons. *ACS Nano* **2010**, *4*, 1259−1278.

DOI: 10.1021/acssuschemeng.5b00724
ACS Sustainable Chem. Eng. XXXX, XXX, XXX−XXX

(47) Ma, Q.; Liu, S.; Weng, L.; Liu, Y.; Liu, B. Growth, structure and photocatalytic properties of hierarchical Cu−Ti−O nanotube arrays by anodization. *J. Alloys Compd.* **2010**, *501*, 333−338.
(48) Slamet; Nasution, H.; Purnama, E.; Kosela, S.; Gunlazuardi, J. Photocatalytic reduction of CO_2 on copper-doped titania catalysts prepared by improved-impregnation method. *Catal. Commun.* **2005**, *6*, 313−319.
(49) Tseng, I.; Chang, W.; Wu, J. Photoreduction of CO_2 Using sol−gel derived titania and titania-supported copper catalysts. *Appl. Catal., B* **2002**, *37*, 37−48.
(50) Tseng, I.; Wu, J.; Chou, H. Effects of sol−gel procedures on the photocatalysis of Cu/TiO_2 in CO_2 photoreduction. *J. Catal.* **2004**, *221*, 432−440.
(51) Li, Y.; Wang, W.; Zhan, Z.; Woo, M.; Wu, C.; Biswas, P. Photocatalytic reduction of CO_2 with H_2O on mesoporous silica supported Cu/TiO_2 catalysts. *Appl. Catal., B* **2010**, *100*, 386−392.
(52) Fang, B.; Kim, J.; Kim, M.; Yu, J. Hierarchical nanostructured carbons with meso-macroporosity: design, characterization and applications. *Acc. Chem. Res.* **2013**, *46*, 1397−1406.
(53) Fang, B.; Kim, M.; Yu, J. Hollow macroporous core/mesoporous shell carbon as highly efficient catalyst support in direct formic acid fuel cell. *Appl. Catal., B* **2008**, *84*, 100−105.
(54) Fang, B.; Kim, J.; Kim, M.; Yu, J. Controllable synthesis of hierarchical nanostructured hollow core/mesopore shell carbon for electrochemical hydrogen storage. *Langmuir* **2008**, *24*, 12068−12072.
(55) Liu, Z.; Bai, H.; Sun, D. Hollow spherical carbon with mesoporous shell as a superb anode catalyst support in proton exchange membrane fuel cell. *Appl. Catal., B* **2011**, *104*, 234−238.
(56) Kim, M.; Fang, B.; Kim, J.; Yang, D.; Kim, Y.; Bae, T.; Yu, J. Ultra-high Li storage capacity achieved by hollow carbon capsule with hierarchical nanoarchitecture. *J. Mater. Chem.* **2011**, *21*, 19362−19367.
(57) Kim, J.; Fang, B.; Song, M.; Yu, J. Topological transformation of thioether-bridged organosilicas into nanostructured functional materials. *Chem. Mater.* **2012**, *24*, 2256−2264.
(58) Fang, B.; Kim, J.; Kim, M.; Bonakdarpour, A.; Lam, A.; Wilkinson, D.; Yu, J. Fabrication of hollow core carbon spheres with hierarchical nanoarchitecture for ultrahigh electrical charge storage. *J. Mater. Chem.* **2012**, *22*, 19031−19038.
(59) Li, H.; Bian, Z.; Zhu, J.; Zhang, D.; Li, G.; Huo, Y.; Li, H.; Lu, Y. Mesoporous titania spheres with tunable chamber structure and enhanced photocatalytic activity. *J. Am. Chem. Soc.* **2007**, *129*, 8406−8407.
(60) Zhao, T.; Liu, Z.; Nakata, K.; Nishimoto, S.; Murakami, T.; Zhao, Y.; Jiang, L.; Fujishima, A. Multichannel TiO_2 hollow fibers with enhanced photocatalytic activity. *J. Mater. Chem.* **2010**, *20*, 5095−5099.
(61) Fang, B.; Kim, J.; Yu, J. Colloid-imprinted carbon with superb nanostructure as an efficient cathode electrocatalyst support in proton exchange membrane fuel cell. *Electrochem. Commun.* **2008**, *10*, 659−662.
(62) Fang, B.; Kim, J.; Kim, M.; Yu, J. Ordered hierarchical nanostructured carbon as a highly efficient cathode catalyst support in proton exchange membrane fuel cell. *Chem. Mater.* **2009**, *21*, 789−796.
(63) Xing, Y.; Fang, B.; Bonakdarpour, A.; Zhang, S.; Wilkinson, D. Facile fabrication of mesoporous carbon nanofibers with unique hierarchical nanoarchitecture for electrochemical hydrogen storage. *Int. J. Hydrogen Energy* **2014**, *39*, 7859−7867.
(64) Sun, X.; Liu, J.; Li, Y. Use of carbonaceous polysaccharide microspheres as templates for fabricating metal oxide hollow spheres. *Chem. - Eur. J.* **2006**, *12*, 2039−2047.
(65) Fang, B.; Kim, M.; Hwang, S.; Yu, J. Colloid-imprinted carbon with tailored nanostructure as an unique anode electrocatalyst support for formic acid oxidation. *Carbon* **2008**, *46*, 876−883.
(66) Kim, J.; Fang, B.; Kim, M.; Yoon, S.; Bae, T.; Ranade, D.; Yu, J. Facile synthesis of mimodal porous silica and multimodal porous carbon as an anode catalyst support in polymer exchange membrane fuel cell. *Electrochim. Acta* **2010**, *55*, 7628−7633.
(67) Xiao, L.; Cao, M.; Mei, D.; Guo, Y.; Yao, L.; Qu, D.; Deng, B. Preparation and electrochemical lithium storage features of TiO_2 hollow spheres. *J. Power Sources* **2013**, *238*, 197−202.
(68) Yu, J.; Guo, H.; Davis, S.; Mann, S. Fabrication of hollow inorganic microspheres by chemically induced self-transformation. *Adv. Funct. Mater.* **2006**, *16*, 2035−2041.
(69) Liu, L.; Gao, F.; Zhao, H.; Li, Y. Tailoring Cu valence and oxygen vacancy in Cu/TiO_2 catalysts for enhanced CO_2 photoreduction efficiency. *Appl. Catal., B* **2013**, *134−135*, 349−358.
(70) Sing, K.; Everett, D.; Haul, R.; Moscou, L.; Pierotti, R.; Rouquerol, J.; Siemieniewska, T. Reporting physisorption data for gas/solid systems with special reference to the determination of surface area and porosity. *Pure Appl. Chem.* **1985**, *57*, 603−619.
(71) Yu, J.; Hai, Y.; Jaroniec, M. Photocatalytic hydrogen production over CuO-modified titania. *J. Colloid Interface Sci.* **2011**, *357*, 223−228.
(72) Wang, X.; Yu, J.; Ho, C.; Hou, Y.; Fu, X. Photocatalytic activity of a hierarchically macro/mesoporous titania. *Langmuir* **2005**, *21*, 2552−2559.
(73) Liu, B.; Nakata, K.; Sakai, M.; Saito, H.; Ochiai, T.; Murakami, T.; Takagi, K.; Fujishima, A. Hierarchical TiO_2 spherical nanostructures with tunable pore size, pore volume, and specific surface area: facile preparation and high-photocatalytic performance. *Catal. Sci. Technol.* **2012**, *2*, 1933−1939.
(74) Fang, B.; Kim, M.; Kim, J.; Song, M.; Wang, Y.; Wang, H.; Wilkinson, D.; Yu, J. High Pt loading on functionalized multiwall carbon nanotube as a highly efficient cathode electrocatalyst for proton exchange membrane fuel cell. *J. Mater. Chem.* **2011**, *21*, 8066−8073.
(75) Fang, B.; Chaudhari, N.; Kim, M.; Kim, J.; Yu, J. Homogeneous deposition of platinum nanoparticles on carbon black for proton exchange membrane fuel cell application. *J. Am. Chem. Soc.* **2009**, *131*, 15330−15338.
(76) Kim, J. H.; Fang, B.; Kim, M.; Yu, J.-S. Hollow spherical carbon with mesoporous shell as a superb anode catalyst support in proton exchange membrane fuel cell. *Catal. Today* **2009**, *146*, 25−30.
(77) Fang, B.; Bonakdarpour, A.; Kim, M.; Kim, J.; Wilkinson, D.; Yu, J. Multimodal porous carbon as a highly efficient electrode material in an EDLC. *Microporous Mesoporous Mater.* **2013**, *182*, 1−7.

DOI: 10.1021/acssuschemeng.5b00724
ACS Sustainable Chem. Eng. XXXX, XXX, XXX−XXX